


Nonvolatile voltage-tunable ferroelectric-superconducting quantum interference memory devices

Journal Article**Author(s):**

Suleiman, Mohammad; Sarott, Martin F.; [Trassin, Morgan](#) ; Badarne, Maria; Ivry, Yachin

Publication date:

2021-09-13

Permanent link:

<https://doi.org/10.3929/ethz-b-000505697>

Rights / license:

[Creative Commons Attribution 4.0 International](#)

Originally published in:

Applied Physics Letters 119(11), <https://doi.org/10.1063/5.0061160>

Funding acknowledgement:

188414 - Multifunctional oxide electronics using natural ferroelectric superlattices (SNF)

This is the author's peer reviewed, accepted manuscript. However, the online version of record will be different from this version once it has been copyedited and typeset.

PLEASE CITE THIS ARTICLE AS DOI: 10.1063/1.50061160

Non-volatile voltage-tunable ferroelectric-superconducting quantum interference memory devices

Mohammad Suleiman,^{1,2} Martin F Sarott,³ Morgan Trassin³, Maria Badarne^{1,2} and Yachin Ivry^{1,2,*}

ORCID:0000-0002-3045-923X

¹ Department of Materials Science and Engineering, Technion – Israel Institute of Technology, Haifa 3200003, Israel.

² Solid State Institute, Technion – Israel Institute of Technology, Haifa 3200003, Israel.

³ Department of Materials, ETH Zurich, Vladimir-Prelog-Weg 4, 8093 Zürich, Switzerland.

*Correspondence to: ivry@technion.ac.il.

Abstract

Superconductivity serves as a unique solid-state platform for electron interference at a device-relevant lengthscale, which is essential for quantum information and sensing technologies. As opposed to semiconducting transistors that are operated by voltage biasing at the nanometer scale, superconductive quantum devices cannot sustain voltage and are operated with magnetic fields, which impose a large device footprint, hindering miniaturization and scalability. Here we introduce a system of superconducting materials and devices that have a common interface with a ferroelectric layer. An amorphous superconductor was chosen for reducing substrate-induced misfit strain and for allowing low-temperature growth. The common quantum pseudowavefunction of the superconducting electrons was controlled by the non-volatile switchable polarization of the ferroelectric by means of voltage biasing. A controllable change of 21% in the critical temperature was demonstrated for a continuous film geometry. Moreover, a controllable change of 54% in the switching current of a superconducting quantum interference device (SQUID) was demonstrated. The ability to voltage bias superconducting devices together with the non-volatile nature of this system paves the way to quantum-based memory devices.

Superconducting quantum interference devices (SQUIDs) are basic building blocks for quantum technologies. The macroscopic quantum characteristic of SQUIDs is advantageous for magnetic sensing,^{1,2} whereas these devices are a major player in the recent race for quantum-information technologies.³⁻⁵ While the perfect conductance of superconductors is advantageous for low power consumption.⁶⁻⁸ following Ohm's law, the absence of resistance also hinders energy efficient voltage biasing. Thus, superconducting quantum devices lack the convenient gating platform that semiconducting transistors have. There has been therefore a continuous effort to introduce tunability to superconductive quantum devices,⁹ including by ionic liquid^{10,11}, as well as by voltage-tunable π -SQUIDs.¹² A prominent example is integration of ferromagnetic components. Ferromagnets retain magnetic polarization, which is switchable with an external magnetic field, allowing non-volatile tunability.^{13,14} Yet, magnetic controllability is more cumbersome than the semiconducting transistor electric-field tunability, especially for miniaturized devices.

Electric tunability of the quantum state of superconductive devices has been demonstrated successfully by introducing a ballistic or very clean semiconductor in proximity to the superconducting device.¹⁵ In several such devices, the gating mechanism is based on voltage-driven charge injection of holes or electrons from the semiconductor either directly or by means of a field effect. The resultant change in the superconductor charge-carrier density (n_s) is accompanied by direct voltage control of the common quantum pseudo-wavefunction of the superconducting electrons: $n_s = |\psi|^2$. Hence, the superconducting energy gap (Δ) is also voltage depended: $\psi = \Delta e^{i\theta}$ (θ is the common phase of the superconductive electrons) as well as material parameters, such as critical temperature (T_c):¹⁶

$$\Delta = 3.66k_B T_c \sqrt{1 - \left(\frac{T}{T_c}\right)^2} \quad (1)$$

Here, k_B is Boltzmann's constant and this relationship is valid for finite temperatures $T \approx T_c$, whereas it is reduced to a simpler form: $\Delta = 1.752k_B T_c$ for $T \rightarrow 0$ K. Likewise, following Ambegaokar and Baratoff,¹⁷ device properties, such as the critical current, are also tunable:

$$I_c = \frac{\pi\Delta}{2q_e R_N} \tanh\left(\frac{\Delta}{2k_B T}\right) \quad (2)$$

where q_e is the electron charge and R_N is the device's normal-state resistance.

This is the author's peer reviewed, accepted manuscript. However, the online version of record will be different from this version once it has been copyedited and typeset.

PLEASE CITE THIS ARTICLE AS DOI: 10.1063/1.50061160

Charge injection with a semiconductor requires constant voltage application and the effect is limited by the charge carrier of the semiconductor. It has been proposed that ferroelectrics offer a potential answer to these two hurdles already from the pioneering work by Ahn *et al.* in 1999.¹⁸ Ferroelectrics are high-dielectric materials that retain electric polarization, which is switchable with an external bias. The internal polarization in ferroelectrics is compensated with a surface charge that is available for direct charge injection^{19,20} as well as induces an electric field.²¹ Here, a layer within the superconductor as thin as the Thomas-Fermi screening length screens the bound charge of the ferroelectric.²²⁻²⁴ The bound charge in the ferroelectric depends on the remanent polarization, which in turn is switchable by an external electric field and is unchanged even upon the field removal due to the hysteretic nature of the ferroelectric polarization. Hence, the superconductor charge density and related parameters change with the polarization switching, giving rise to an effective non-volatile memory effect of the superconducting properties (see Figure 1A-B).

Despite the great potential of ferroelectric-superconductive quantum devices, to date, only a handful number of successful attempts have been demonstrated.^{25,26} Similar to ferromagnetic and semiconducting tunability, the main challenge in realizing competitive ferroelectric-superconducting quantum devices is the limited capability of presenting an electronically transparent interface between the two materials. That is, the existence of chemical, electric, and magnetic impurities as well as strain at the interface impinges charge control in the superconductor, suppressing the voltage tunability. Thus far, to overcome these limitations, the superconducting and ferroelectric materials were selected according to the match of their lattice parameters. However, this approach is limited to high- T_c superconductors^{25,26} and superconductors with an extremely low T_c . Another approach uses 2D superconductors, where the material itself is the interface.²⁷ Nevertheless, contemporary quantum-information technologies are based on thin superconductors with a finite thickness and with T_c in the range of $\sim 1-10$ K.²⁸⁻³¹ Consequently, although a ferroelectric-based voltage-tunable Josephson junction has been demonstrated (for high- T_c superconductors), the effort thus far has been put in modifying T_c of a continuous film and not in controlling the properties of a SQUID.

Here, we present non-volatile voltage-tunability of the critical temperature of a 15 nm continuous superconductive amorphous molybdenum silicide film that was deposited on a 70-nm

This is the author's peer reviewed, accepted manuscript. However, the online version of record will be different from this version once it has been copyedited and typeset.

PLEASE CITE THIS ARTICLE AS DOI: 10.1063/5.0061160

thick $\text{PbZr}_{0.2}\text{Ti}_{0.8}\text{O}_3$ film on a 15-nm SrRuO_3 bottom electrode. This effect was then used for demonstrating voltage-tunable SQUID with a memory effect.

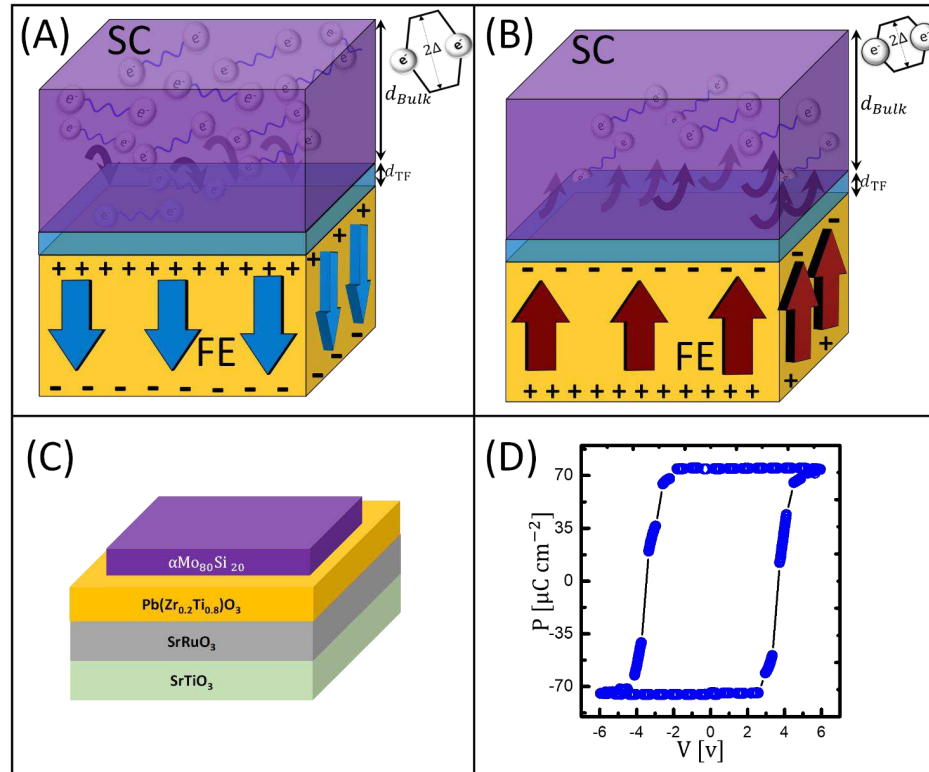


FIG. 1. The superconductive-ferroelectric system. (A) Negative polarization in the ferroelectric gives rise to a bound charge at the superconducting-ferroelectric surface that is compensated by a screening layer of a thickness d_{TF} . The corresponding change in charge-carrier density affects the superconducting energy gap and related properties. (B) An opposite effect occurs with positive polarization. (C) $\alpha\text{Mo}_{80}\text{Si}_{20}$ was deposited on top of a lead zirconate titanate (PZT) ferroelectric film, which in turn was laid on a bottom SrRuO_3 on a SrTiO_3 substrate. The three oxide layers form an epitaxy structure with a good lattice matching between them, whereas the amorphous structure of the superconductors allows an electronically clean interface with the ferroelectric. (D) Polarization hysteresis cycle of the ferroelectric. Polarization hysteresis curve of the PZT, showing remnant polarization of $75 \mu\text{C cm}^{-2}$ and 4 V coercivity.

This is the author's peer reviewed, accepted manuscript. However, the online version of record will be different from this version once it has been copyedited and typeset.

PLEASE CITE THIS ARTICLE AS DOI: 10.1063/1.50061160

An $\alpha\text{Mo}_{80}\text{Si}_{20}$ was deposited by means of magnetron sputtering on top of a lead zirconate titanate (PZT) ferroelectric film, which in turn was laid on a bottom electrode as illustrated schematically in Figure 1C (see methods for details regarding the material processing). Amorphous materials do not require lattice matching.^{31,32} PZT was chosen because the associated bound charge ($4.33 \cdot 10^{-3}$ charge carriers per unit cell³³ is much larger than the available charge in semiconducting material ($1.8 \cdot 10^{-4}$ charge carriers per unit cell for highly doped silicon).³⁴ Using piezoresponse force microscopy, it was found that the polarization in the ferroelectric is reversible with a bias of 5-6 V (Figure 1D). Thus, a higher voltage bias (10 V) was applied for 10 min to switch the ferroelectric polarization at the substrate sandwiched between the bottom electrode and the $\alpha\text{Mo}_{80}\text{Si}_{20}$ films at the normal state ($T=25$ K). The resultant effect on the superconducting T_c was then measured by removing the bias and cooling down the polarized sample. The sample was then heated back to the normal state ($T=25$ K) and the polarization was switched with an opposite bias before T_c was measured again. This experimental procedure was performed repeatedly to verify the effect reproducibility. Here, T_c was determined by the temperature at which the resistance drops by 90% from its value at 20 K. This experimental protocol is demonstrated schematically in Figure 2A. To demonstrate the repeatability of the process, a sequential cycle was performed. Figure 2B shows that a negative polarization in the ferroelectric was accompanied by $T_c = 6.8 \pm 0.1$ K, whereas $T_c = 5.8 \pm 0.1$ K for positive polarization.

This is the author's peer reviewed, accepted manuscript. However, the online version of record will be different from this version once it has been copyedited and typeset.

PLEASE CITE THIS ARTICLE AS DOI: 10.1063/5.0061160

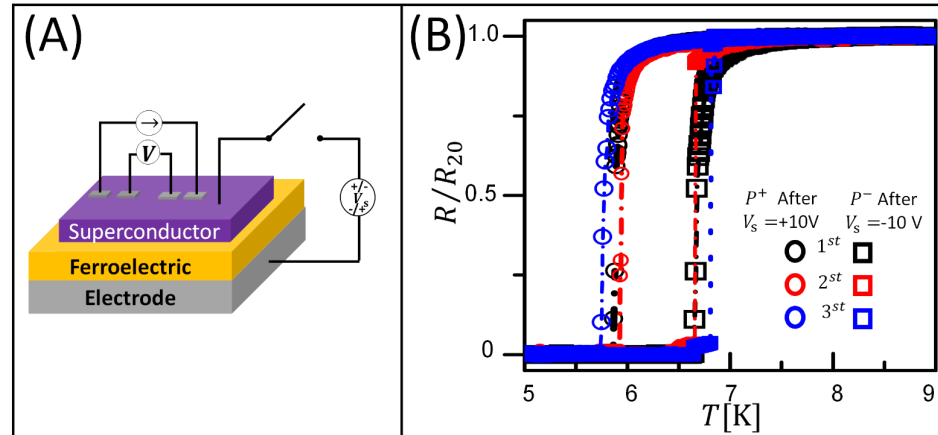


FIG. 2. Voltage-tunable superconductive-ferroelectric device. (A) Schematics of the T_c measurement setup. The polarization was first set by biasing the ferroelectric with V_s that is larger than the coercive value with either positive or negative polarity. After removing the bias, T_c was extracted from a four-point measurement. The procedure was then repeated for the opposite polarity. (B) Cooling curves of $\alpha\text{Mo}_{80}\text{Si}_{20}$ on a ferroelectric substrate shows that the measured T_c at 90% drop of the resistance was 5.7 K for positive polarization (circles) and 6.9 K for negative polarization (squares) as well as the reproducibility of the effect for three sequencing cycles (black, blue and red curves).

To demonstrate the direct effect of polarization reversal on the behavior of a SQUID, a planar SQUID was fabricated as illustrated in Figure 3 (see Reference³⁵ for details related to device fabrication). Figure 4 shows that a negative polarization in the ferroelectric resulted in $I_c = 4.0 \pm 0.03 \mu\text{A}$, and $I_c = 2.6 \pm 0.03 \mu\text{A}$ for positive polarization (measured at 3 K). These values correspond in a good agreement to the estimated change in I_c based on the measured change in T_c , following Equations 1-2. That is, the SQUID characteristics are voltage-tunable with a measurable change of 54%, whereas the effect is observed even after the voltage is removed.

This is the author's peer reviewed, accepted manuscript. However, the online version of record will be different from this version once it has been copyedited and typeset.

PLEASE CITE THIS ARTICLE AS DOI: 10.1063/5.0061160

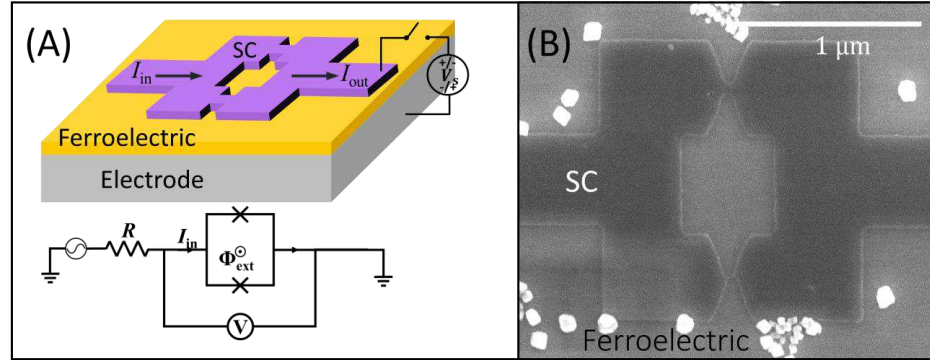


FIG. 3. Non-volatile voltage-gated SQUID. (A) Schematics of a SQUID with current circulating in a loop that contains two parallel weak links on top of a ferroelectric substrate with switchable polarization. (B) Electron micrograph of 15-nm thick planar $\alpha\text{Mo}_{80}\text{Si}_{20}$ SQUIDs on a ferroelectric substrate.

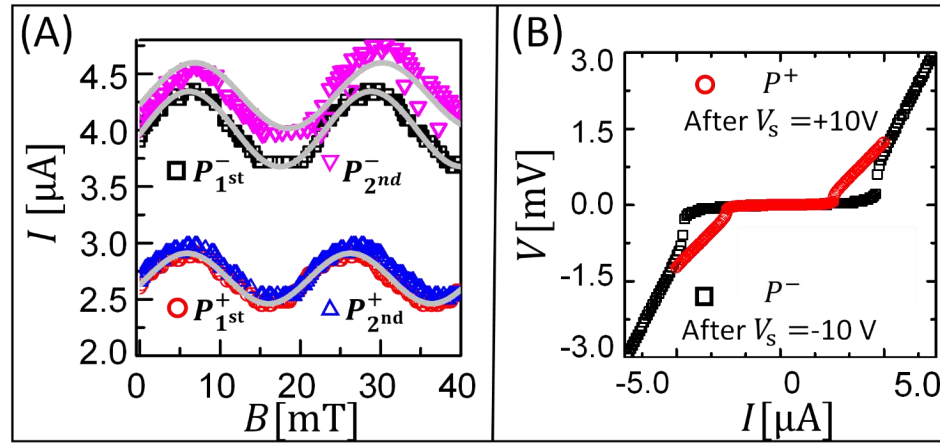


FIG. 4. (A) Interference signal of a planar $\alpha\text{Mo}_{80}\text{Si}_{20}$ SQUID showing a shift of the switching current as a result of polarization reversal in the ferroelectric film upon which the SQUID is laid. Gray curves correspond to the best fit of a sine (see Table S1) (B) Current-voltage curves of the $\alpha\text{Mo}_{80}\text{Si}_{20}$ SQUID at zero magnetic field measured for negative and positive polarization of the ferroelectric, showing a significant change in both I_c (length of the horizontal segment) as well as the device's normal resistance (slope of the linear regime at the normal state). Results of two sequencing measurements are presented, demonstrating the reproducibility of the effect (the derivative resistance is depicted in Figure S3).

To complement the device and material characterization, the device normal resistance and the superconducting charge-carrier density were also measured for negative and positive ferroelectric polarization. Table 1 summarizes the tunable properties of both the continuous film and the device. Substituting the two values of T_c and the measurement temperature ($T = 3$ K) in Equation 1 and substituting the resultant energy gap as well as the other relevant values in Equation 2, the obtained I_c values show a similar trend of enhanced tunability with respect to T_c . Yet, note that a small discrepancy between the calculated and measured values of I_c is expected due to, *e.g.*, a measurement temperature within the range $T_c > T > 0$ K and a possible difference between the film's T_c and the critical temperature of the device.

The effect of polarization reversal on n_e can also be calculated. The surface charge due to ferroelectric remnant polarization (P_r) satisfies: $Q_{\text{surf}} = \oint P_r \cdot dA$, Where A is surface area. Thus, the change in surface charge due to polarization reversal is given by: $\delta Q_{\text{surf}} = 2AP_r$. It is now possible to substitute $A = 6000 \text{ nm}^2$ for the weak links of the above SQUID (Figure 3B) and $P_r = 75 \text{ } \mu\text{C cm}^{-2}$ for the PZT (see Figure 1D) to obtain that the change in charge carrier density in the 15-nm thick $\alpha\text{Mo}_{80}\text{Si}_{20}$ film due to polarization reversal is: $\delta n_e \approx 5 \cdot 10^{26} \text{ m}^{-3}$.

The Thomas-Fermi screening length of αMoSi is about one tenth of the thickness of the films examined in this work.³⁶ Yet, the device thickness is comparable to the coherence length ($< 3\xi$). In this geometry, we expect the electron-phonon coupling and the density of states do not vary much between the screening layer and the bulk.²⁴

Hall-effect measurements of the $\alpha\text{Mo}_{80}\text{Si}_{20}$ film were performed for a negative and a positive polarized ferroelectric for extracting the corresponding change in charge carriers within the superconductor (Figure S4). The Hall coefficient is extracted from the slope of the measured Hall resistivity (ρ_{xy}) with respect to magnetic field at the normal state. We obtained Hall coefficients of 4.2 and $9 \cdot 10^{-8} \text{ } \Omega \cdot \text{m T}^{-1}$ and therefore charge-carrier density of 15 and $7 \cdot 10^{25} \text{ m}^{-3}$ for the respective positive and negative polarizations. Thus, the change in charge-carrier density due to polarization reversal is $8 \cdot 10^{25} \text{ m}^{-3}$, which is in agreement with the expected charge that is required for polarization screening.³⁷⁻³⁹ Table 1 shows that the extracted δn_e is in agreement with the expected value, where it also presents the extracted coherence length $\xi = \frac{\hbar v_F}{\pi \Delta}$ (with Fermi velocity

of $v_F \approx 3 \cdot 10^4 \text{ m s}^{-1}$ for molybdenum silicide⁴⁰ and \hbar is the reduced Planck's constant), SQUID's figure of merit $\beta_L = \frac{2I_c L}{\Phi_0}$, ($L = 8.035 \cdot 10^{-10} \text{ [H]}$ is the device inductance and Φ_0 is magnetic flux quantum)^{16,35} for the two polarization states.

Polarization state	T_c [K]	I_c [μA]	β_L	R_n [Ω]	ξ [nm]	n_e [10^{25} m^{-3}]	2Δ [meV]
P^+	5.8 ± 0.1	2.6 ± 0.05	2.0 ± 0.1	1750 ± 50	6 ± 0.1	7 ± 0.5	2.1 ± 0.1
P^-	6.8 ± 0.1	4.0 ± 0.05	3.1 ± 0.1	950 ± 50	4.5 ± 0.1	15 ± 0.5	2.7 ± 0.1

Table 1| Effects of polarization on superconductive film and device properties.

Therefore, to conclude, the change in material and device parameters can be attributed directly to the polarization-induced charge injection as elucidated schematically in Figure 1A-B, demonstrating non-volatile memory effect of the superconductive quantum material and devices.

Supplementary Material

See the supplementary material for the materials and methods, topography and in-plane polarization of the ferroelectric substrate, crystallography analysis of the substrate, effects of ferroelectric polarization on differential $\alpha\text{Mo}_{80}\text{Si}_{20}$ resistance, Hall resistance for negative and positive ferroelectric polarization and Fitting value for Interference signal of a planar $\alpha\text{Mo}_{80}\text{Si}_{20}$ SQUID

Acknowledgments: The authors acknowledge financial support from the Israel Science Foundation (ISF) grants number 1602/17 and Pazy Research Foundation grant #149-2020, the Zuckerman STEM Leadership Program, the Technion Russell Barry Nanoscience Institute and the Technion Microelectronic Center. We thank the following personnel for technical support: Dr. Guy Ankonina (sputtering and ellipsometry); Dr. Adi Goldner (device fabrication); Dr. Olga Kleinerman (SEM) as well as Dr. Anna Eyal from the Technion's Quantum Materials Research Center (low-temperature measurements). Finally, we thank Prof. Karen Michaeli and Prof. Emanuele G. Dalla Torre for fruitful discussions.

This is the author's peer reviewed, accepted manuscript. However, the online version of record will be different from this version once it has been copyedited and typeset.

PLEASE CITE THIS ARTICLE AS DOI: 10.1063/5.0061160

Data Availability

The data that support the findings of this study are available within this article (and its supplementary material). Further data are available from the corresponding author upon reasonable request.

Reference

- ¹ K. Wiesenfeld and F. Moss, *Nature* **373**, 33 (1995).
- ² M. Suleiman, E.G.D. Torre, and Y. Ivry, *Arxiv* **10297**, (2020).
- ³ B.M. Hynek, R.E. Arvidson, and R.J. Phillips, *J. Geophys. Res. E Planets* **107**, 159 (2002).
- ⁴ Z. Zhou, S.I. Chu, and S. Han, *Phys. Rev. B - Condens. Matter Mater. Phys.* **66**, 1 (2002).
- ⁵ S. Popescu, N. Linden, and R. Jozsa, *J. Phys. A. Math. Gen.* **34**, 6723 (2001).
- ⁶ A.N. McCaughan, V.B. Verma, S.M. Buckley, J.P. Allmaras, A.G. Kozorezov, A.N. Tait, S.W. Nam, and J.M. Shainline, *Nat. Electron.* **2**, 451 (2019).
- ⁷ N. Takeuchi, Y. Yamanashi, and N. Yoshikawa, *Supercond. Sci. Technol.* **28**, (2015).
- ⁸ H. Hayakawa, N. Yoshikawa, S. Yorozu, and A. Fujimaki, *Proc. IEEE* **92**, 1549 (2004).
- ⁹ R. Winik, I. Holzman, E.G. Dalla Torre, E. Buks, and Y. Ivry, *Appl. Phys. Lett.* **112**, 122601 (2018).
- ¹⁰ D. Costanzo, H. Zhang, B.A. Reddy, H. Berger, and A.F. Morpurgo, *Nat. Nanotechnol.* **13**, 483 (2018).
- ¹¹ H. Zhang, C. Berthod, H. Berger, T. Giamarchi, and A.F. Morpurgo, *Nano Lett.* **19**, 8836 (2019).
- ¹² H. Atesci, W. Gelling, F. Coneri, H. Hilgenkamp, and J.M. Van Ruitenbeek, *Int. J. Mol. Sci.* **19**, (2018).
- ¹³ A. Chernyshov, M. Overby, X. Liu, J.K. Furdyna, Y. Lyanda-Geller, and L.P. Rokhinson, *Nat. Phys.* **5**, 656 (2009).

This is the author's peer reviewed, accepted manuscript. However, the online version of record will be different from this version once it has been copyedited and typeset.

PLEASE CITE THIS ARTICLE AS DOI: 10.1063/5.0061160

- ¹⁴ M. Liu, T. Nan, J.M. Hu, S.S. Zhao, Z. Zhou, C.Y. Wang, Z. De Jiang, W. Ren, Z.G. Ye, L.Q. Chen, and N.X. Sun, *NPG Asia Mater.* **8**, 316 (2016).
- ¹⁵ E. Mönch, D.A. Bandurin, I.A. Dmitriev, I.Y. Phinney, I. Yahniuk, T. Taniguchi, K. Watanabe, P. Jarillo-Herrero, and S.D. Ganichev, *Nano Lett.* **20**, 5943 (2020).
- ¹⁶ M. Tinkham, *Introduction to Superconductivity*, 2nd ed (Mineola, N.Y : Dover, 2004).
- ¹⁷ V. Ambegaokar and A. Baratoff, *Phys. Rev. Lett.* **11**, 104 (1963).
- ¹⁸ C.H. Ahn, S. Gariglio, P. Paruch, T. Tybell, L. Antognazza, and J.M. Triscone, *Science*. **284**, 1152 (1999).
- ¹⁹ Q. Huang, Z. Chen, M.J. Cabral, F. Wang, S. Zhang, F. Li, Y. Li, S.P. Ringer, H. Luo, Y.W. Mai, and X. Liao, *Nat. Commun.* **12**, 1 (2021).
- ²⁰ C.M. Teodorescu, *Phys. Chem. Chem. Phys.* **23**, 4085 (2021).
- ²¹ X. Gao and Z. Zhao, *Sci. China Chem.* **58**, 947 (2015).
- ²² E. Piatti, D. Daghero, G.A. Ummarino, F. Laviano, J.R. Nair, R. Cristiano, A. Casaburi, C. Portesi, A. Sola, and R.S. Gonnelli, *Phys. Rev. B* **95**, 1 (2017).
- ²³ G.A. Ummarino, E. Piatti, D. Daghero, R.S. Gonnelli, I.Y. Sklyadneva, E. V. Chulkov, and R. Heid, *Phys. Rev. B* **96**, 1 (2017).
- ²⁴ E. Piatti, *Nano Express* **2**, 024003 (2021).
- ²⁵ A. Crassous, R. Bernard, S. Fusil, K. Bouzouane, D. Le Bourdais, S. Enouz-Vedrenne, J. Briatico, M. Bibes, A. Barthélémy, and J.E. Villegas, *Phys. Rev. Lett.* **107**, 1 (2011).
- ²⁶ A. Crassous, R. Bernard, S. Fusil, K. Bouzouane, J. Briatico, M. Bibes, A. Barthélémy, and J.E. Villegas, *J. Appl. Phys.* **113**, 024910 (2013).
- ²⁷ K.S. Takahashi, M. Gabay, D. Jaccard, K. Shibuya, T. Ohnishi, M. Lippmaa, and J.-M. Triscone, *Nature* **441**, 195 (2006).
- ²⁸ J. Kelly, R. Barends, A.G. Fowler, A. Megrant, E. Jeffrey, T.C. White, D. Sank, J.Y. Mutus, B. Campbell, Y. Chen, Z. Chen, B. Chiaro, A. Dunsworth, I.C. Hoi, C. Neill, P.J.J. O'Malley, C. Quintana, P. Roushan, A. Vainsencher, J. Wenner, A.N. Cleland, and J.M. Martinis, *Nature* **519**,

This is the author's peer reviewed, accepted manuscript. However, the online version of record will be different from this version once it has been copyedited and typeset.

PLEASE CITE THIS ARTICLE AS DOI: 10.1063/5.0061160

66 (2015).

²⁹ J. Clarke and F.K. Wilhelm, *Nature* **453**, 1031 (2008).

³⁰ F. Arute, K. Arya, R. Babbush, D. Bacon, J.C. Bardin, R. Barends, R. Biswas, S. Boixo, F.G.S.L. Brandao, D.A. Buell, B. Burkett, Y. Chen, Z. Chen, B. Chiaro, R. Collins, W. Courtney, A. Dunsworth, E. Farhi, B. Foxen, A. Fowler, C. Gidney, M. Giustina, R. Graff, K. Guerin, S. Habegger, M.P. Harrigan, M.J. Hartmann, A. Ho, M. Hoffmann, T. Huang, T.S. Humble, S. V. Isakov, E. Jeffrey, Z. Jiang, D. Kafri, K. Kechedzhi, J. Kelly, P. V. Klimov, S. Knysh, A. Korotkov, F. Kostritsa, D. Landhuis, M. Lindmark, E. Lucero, D. Lyakh, S. Mandrà, J.R. McClean, M. McEwen, A. Megrant, X. Mi, K. Michielsen, M. Mohseni, J. Mutus, O. Naaman, M. Neeley, C. Neill, M.Y. Niu, E. Ostby, A. Petukhov, J.C. Platt, C. Quintana, E.G. Rieffel, P. Roushan, N.C. Rubin, D. Sank, K.J. Satzinger, V. Smelyanskiy, K.J. Sung, M.D. Trevithick, A. Vainsencher, B. Villalonga, T. White, Z.J. Yao, P. Yeh, A. Zalcman, H. Neven, and J.M. Martinis, *Nature* **574**, 505 (2019).

³¹ Y. Ivry, J.J. Surick, M. Barzilay, C.S. Kim, F. Najafi, E. Kalfon-Cohen, A.D. Dane, and K.K. Berggren, *Nanotechnology* **28**, 435205 (2017).

³² I. Holzman and Y. Ivry, *Adv. Quantum Technol.* **2**, 1800058 (2019).

³³ P.E. Janolin, B. Fraisse, F. Le Marrec, and B. Dkhil, *Appl. Phys. Lett.* **90**, 1 (2007).

³⁴ B.Y.L. Epitaxy, V. Epitaxy, G. Techniques, P.F. Fewster, and A.F.W. Willoughby, **50**, 648 (1980).

³⁵ I. Holzman and Y. Ivry, *AIP Adv.* **9**, 105028 (2019).

³⁶ A. Banerjee, L.J. Baker, A. Doye, M. Nord, R.M. Heath, K. Erotokritou, D. Bosworth, Z.H. Barber, I. MacLaren, and R.H. Hadfield, *Supercond. Sci. Technol.* **30**, (2017).

³⁷ S.P. Chockalingam, M. Chand, J. Jesudasan, V. Tripathi, and P. Raychaudhuri, *Phys. Rev. B - Condens. Matter Mater. Phys.* **77**, 214503 (2008).

³⁸ N.P. Breznay, K. Michaeli, K.S. Tikhonov, A.M. Finkel'stein, M. Tendulkar, and A. Kapitulnik, *Phys. Rev. B - Condens. Matter Mater. Phys.* **86**, 014514 (2012).

³⁹ J.W.C. De Vries and A.H. Van Ommen, *J. Appl. Phys.* **64**, 749 (1988).



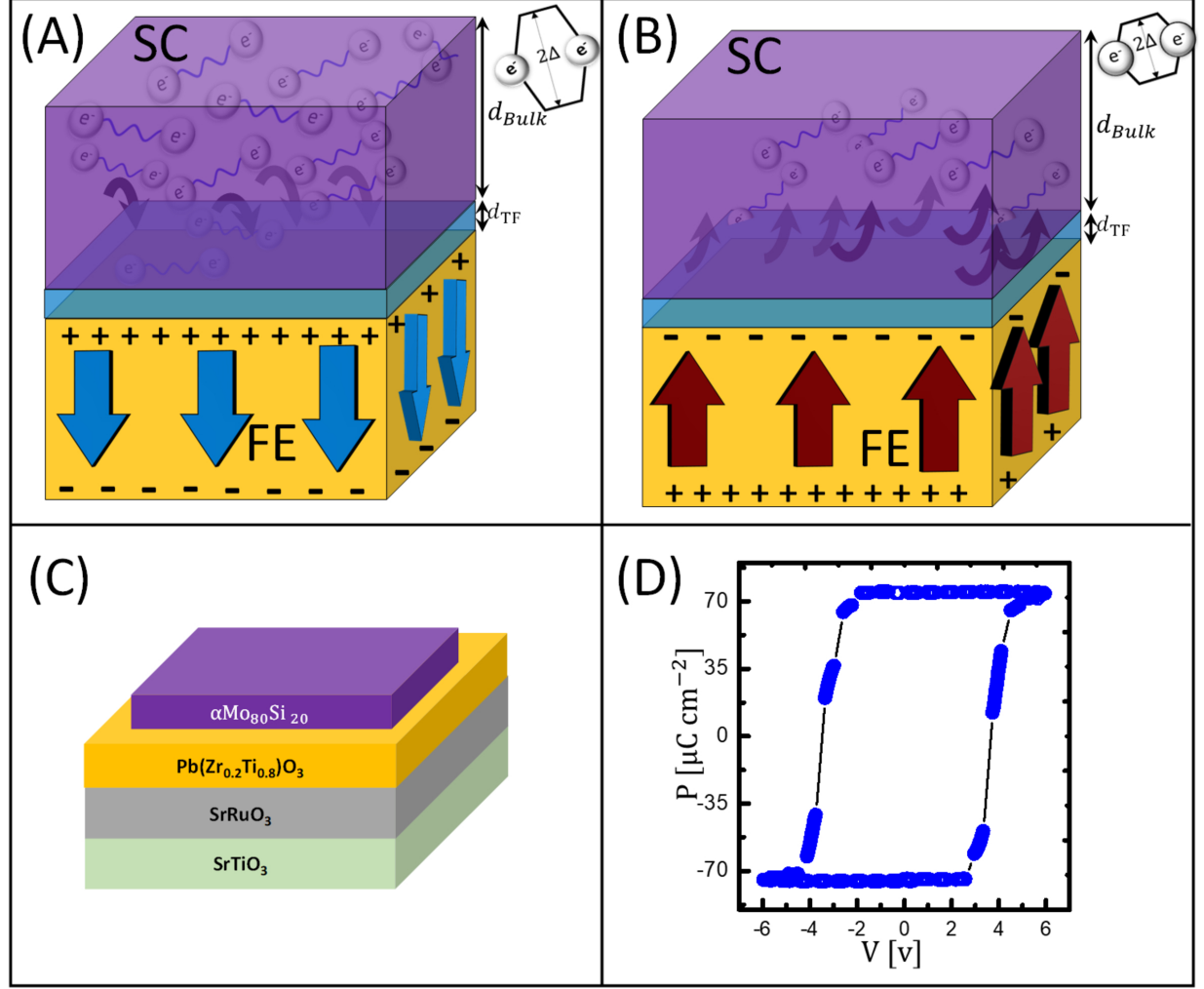
This is the author's peer reviewed, accepted manuscript. However, the online version of record will be different from this version once it has been copyedited and typeset.

PLEASE CITE THIS ARTICLE AS DOI: 10.1063/1.50061160

⁴⁰ J.S. Lehtinen, A. Kemppinen, E. Mykkänen, M. Prunnila, and A.J. Manninen, *Supercond. Sci. Technol.* **31**, (2018).

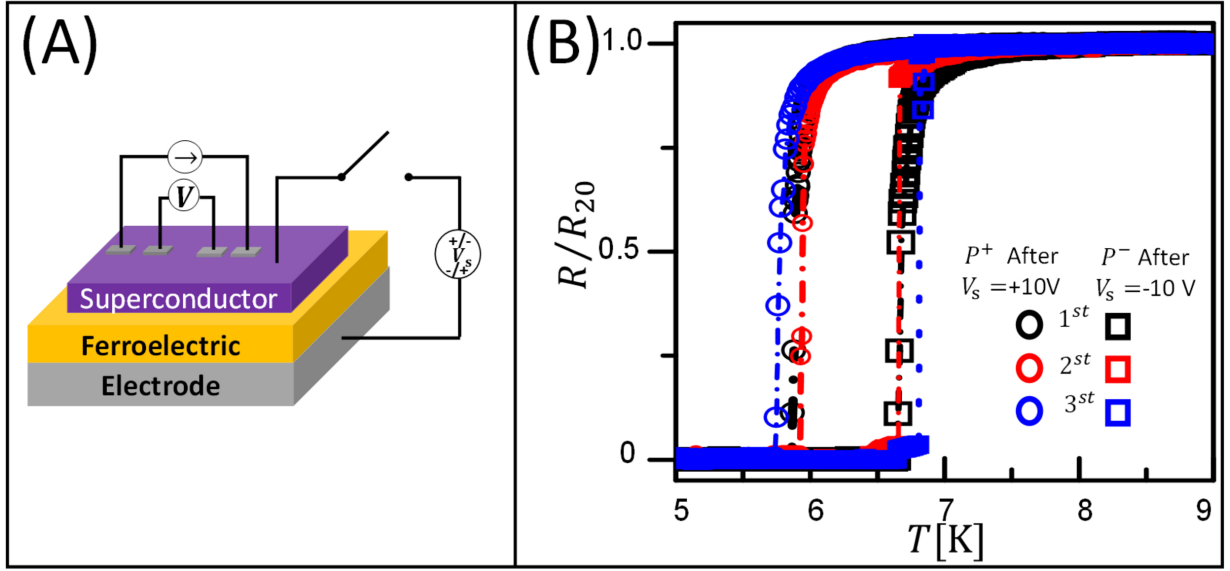
This is the author's peer reviewed, accepted manuscript. However, the online version of record will be different from this version once it has been copyedited and typeset.

PLEASE CITE THIS ARTICLE AS DOI: 10.1063/1.50061160



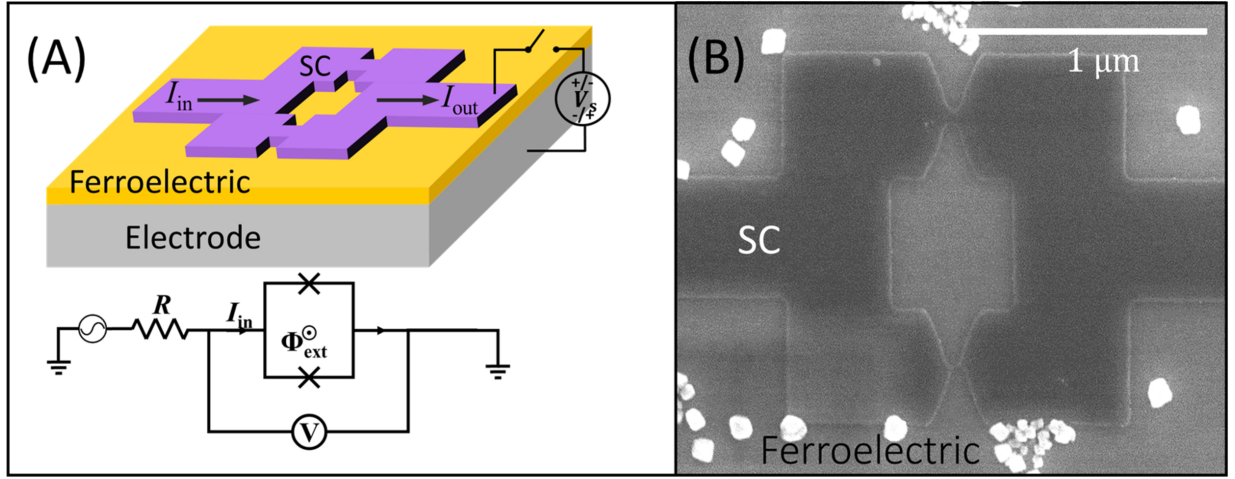
This is the author's peer reviewed, accepted manuscript. However, the online version of record will be different from this version once it has been copyedited and typeset.

PLEASE CITE THIS ARTICLE AS DOI: 10.1063/5.0061160



This is the author's peer reviewed, accepted manuscript. However, the online version of record will be different from this version once it has been copyedited and typeset.

PLEASE CITE THIS ARTICLE AS DOI: 10.1063/1.50061160



This is the author's peer reviewed, accepted manuscript. However, the online version of record will be different from this version once it has been copyedited and typeset.

PLEASE CITE THIS ARTICLE AS DOI: 10.1063/5.0061160

